# A dynamical classification of the cosmic web

## J. E. Forero-Romero,[1]⋆ Y. Hoffman,[2] S. Gottlöber,[1] A. Klypin[3] and G. Yepes[4]

[1]*Astrophysikalisches Institut Potsdam, An der Sternwarte 16, D-14482 Potsdam, Germany*
[2]*Racah Institute of Physics, Hebrew University, Jerusalem 91904, Israel*
[3]*Department of Astronomy, New Mexico State University, Box 30001, Department 4500, Las Cruces, NM 880003, USA*
[4]*Grupo de Astrofísica, Universidad Autónoma de Madrid, Madrid E-28049, Spain*

**ABSTRACT**

In this paper, we propose a new dynamical classification of the cosmic web. Each point in space is classified in one of four possible web types: voids, sheets, filaments and knots. The classification is based on the evaluation of the deformation tensor (i.e. the Hessian of the gravitational potential) on a grid. The classification is based on counting the number of eigenvalues above a certain threshold, $\lambda_{th}$, at each grid point, where the case of zero, one, two or three such eigenvalues corresponds to void, sheet, filament or a knot grid point. The collection of neighbouring grid points, friends of friends, of the same web type constitutes voids, sheets, filaments and knots as extended web objects.

A simple dynamical consideration of the emergence of the web suggests that the threshold should not be null, as in previous implementations of the algorithm. A detailed dynamical analysis would have found different threshold values for the collapse of sheets, filaments and knots. Short of such an analysis a phenomenological approach has been opted for, looking for a single threshold to be determined by analysing numerical simulations.

Our cosmic web classification has been applied and tested against a suite of large (dark matter only) cosmological *N*-body simulations. In particular, the dependence of the volume and mass filling fractions on $\lambda_{th}$ and on the resolution has been calculated for the four web types. We also study the percolation properties of voids and filaments.

Our main findings are as follows. (i) Already at $\lambda_{th} = 0.1$ the resulting web classification reproduces the visual impression of the cosmic web. (ii) Between $0.2 \lesssim \lambda_{th} \lesssim 0.4$, a system of percolated voids coexists with a net of interconnected filaments. This suggests a reasonable choice for $\lambda_{th}$ as the parameter that defines the cosmic web. (iii) The dynamical nature of the suggested classification provides a robust framework for incorporating environmental information into galaxy formation models, and in particular to semi-analytical models.

**Key words:** methods: numerical – cosmology: large-scale structure of Universe.

## 1 INTRODUCTION

The large-scale structure of the Universe, as depicted from galaxy surveys, weak lensing maps and numerical simulations, shows a web of three-dimensional structures. There are three features that can be generally observed. First, most of the volume resides in underdense regions, secondly most of the volume is permeated by filaments, thirdly the densest clumps are located at the intersection of filaments (Bond, Kofman & Pogosyan 1996). This motivates a classification of the cosmic web into at least three categories: voids (underdense regions), filaments and knots (densest clumps).

There is clear evidence that certain observed properties of galaxies correlate with their environments. For example, the morphology density relation stipulates that elliptical galaxies are found preferentially in crowded environments and spiral galaxies are found in the field (Dressler 1980). The same kind of correlation can be found in terms of the colours of the galaxies (Blanton et al. 2005), star formation history and ages.

According to the current paradigm of structure formation, galaxies form and evolve in dark matter (DM) haloes (White & Rees 1978). It follows that the study of such environmental dependence should commence with the effort to understand the formation of DM haloes in the context of the cosmic web (Avila-Reese et al. 2005; Gao, Springel & White 2005; Maulbetsch et al. 2007). This motivates us to search for a robust and meaningful method to classify the different environments in numerical simulations. Such a

⋆E-mail: jforero@aip.de

classification should provide the framework for studying the environmental dependence of galaxy formation.

Translating the visual impression into an algorithm that classifies the local geometry into different environments is not a trivial task. A somewhat less challenging, yet very closely related, task is that of identifying just the voids out of the cosmic web. A thorough review and comparison of different algorithms of void finders has been recently presented in Colberg et al. (2008). The void finders can be classified according to the method employed. Most are based on the point distribution of galaxies or haloes while others are based on the smoothed density or potential fields. Some of the finders are based on spherical filters while others assume no inherent symmetry (Arbabi-Bidgoli & Müller 2002; Plionis & Basilakos 2002; Gottlöber et al. 2003; Colberg et al. 2005; Shandarin et al. 2006; Brunino et al. 2007; Platen, van de Weygaert & Jones 2007; Neyrinck 2008).

It should be emphasized that an environment finder should be evaluated by its merits and it cannot be labelled as right or wrong. A good algorithm should provide a quantitative classification which agrees with the visual impression and it should be based on a robust and well-defined numerical scheme. Yet, it is desirable for an algorithm to be based on simple physical considerations so that its outcome can be estimated analytically. Also, simplicity is always very highly desired.

A variety of approaches have been employed in the classification of the cosmic environment into its basic elements. The simplest way is based on the association of the environment with the local density, evaluated with a top-hat filter of some width (Lemson & Kauffmann 1999). The density field can be analysed in a much more sophisticated and elaborated way. This is the case of the web classification based on the multiscale analysis of the Hessian matrix of the density field (Aragón-Calvo et al. 2007) or the skeleton analysis of the density field (Novikov, Colombi & Doré 2006; Sousbie et al. 2008). Both methods classify the cosmic web by pure geometrical tools applied to the density field. A very different approach is done within a dynamical framework in which the analysis of the gravitational potential is used to classify the web. This has been inspired by the seminal work of Zeldovich (1970) that led to the 'Russian school of structure formation' (e.g. Arnold, Shandarin & Zeldovich 1982; Klypin & Shandarin 1983). The quasi-linear theory of the Zeldovich approximation predicts the existence of an infinitely connected web of pancakes (i.e. sheets), filaments and knots. This morphological classification is based on the study of the eigenvalues of the deformation tensor, namely the Hessian matrix of the linear gravitational field.

A recent application of the Zeldovich-based classification has been provided by Lee & Lee (2008) who used a Wiener filter linear reconstruction of the local density field and evaluated the linear deformation, and hence also the shear, tensor on a grid. The cosmic web has been classified according the structure of the shear tensor.

A different approach has been followed by Hahn et al. (2007) who suggested that the full non-linear gravitational potential should be used for the geometrical classification. Apart from the difference between the linear and the non-linear potential, both Hahn et al. (2007) and Lee & Lee (2008) use the same scheme. Namely, the Hessian of the gravitational potential is evaluated on a grid and its eigenvalues are examined locally.

The Hahn et al. (2007) algorithm provides a very attractive approach to the classification of the cosmic web. We find the dynamical basis of the algorithm to be its main virtue. The cosmic web is essentially imprinted by the gravitational field induced by the distribution of the DM already in the linear regime, as it is clearly manifested by

the Zeldovich (1970) approximation. Now, it is true that the cosmic web can be classified and analysed in a variety of ways and the choice of the particular method should depend on the problem one attempts to address. Yet, it is gravity that governs the emergence of the large-scale structure and drives the formation of galaxies embedded within the cosmic web. It seems therefore most appropriate to define the web by its dynamical properties. This drives us to follow the earlier Hahn et al. approach and extend it. These authors classified the web characteristic by adopting a zero threshold for the eigenvalues. Our approach is to consider a non-zero threshold and examine what value best matches visual appearance and other web characteristics as exhibited by *N*-body simulations.

The approach adopted by Hahn et al. (2007) and followed here is that each point in space is assigned a property defined here as a web type. Namely, a web type is classified as a void, sheet, filament or knot according to the number of eigenvalues above a given threshold. It is the collective classification of all points in space which gives rise to the geometrical construction we call the cosmic web.

The collection of all neighbouring points, say in the sense of friends of friends (FoF), of a given web type defines web objects of that types. For example, the collection of neighbouring void points constitutes a void.

This paper is organized as follows. The web classification scheme is described in Section 2. The *N*-body simulation used in the paper and the numerical implementation of the web classification are presented in Section 3. Section 4 describes the main properties of the cosmic web and in particular its dependence on the smoothing scale and the free parameter of our classification scheme. Section 5 concentrates on the properties of the voids sector of the cosmic web. Section 6 studies the fragmentation of filaments in order to give a confidence interval to the free parameter that was introduced. In Section 7, we revisit the Sections 4 and 5 to study the effect of cosmic variance. The paper concludes with a general discussion and a summary of the main results of the paper (Section 8).

## 2  WEB CLASSIFICATION

Hahn et al. (2007) have recently suggested a new dynamical classification of the cosmic web. The basic idea of their approach is that the eigenvalues of the deformation tensor determine the geometrical nature of each point in space.

The deformation tensor, $T_{\alpha\beta}$, is defined by the Hessian of the gravitational potential $\phi$:

$$T_{\alpha\beta} = \frac{\partial^2 \phi}{\partial r_\alpha \partial r_\beta}. \tag{1}$$

The definition of the deformation tensor[1] explicitly assumes that the matter density field is known and that it is smoothed with a finite kernel, which is introduced in order to control the high-frequency behaviour of the calculated derivatives. For simplicity, the smoothed density field is defined over a (Cartesian) grid.

Hahn et al. (2007) considered the three eigenvalues of the deformation tensor, $\tilde{\lambda}_1 \geq \tilde{\lambda}_2 \geq \tilde{\lambda}_3$, and classified a grid point according the number of positive eigenvalues at that point. Namely, a void point corresponds to no positive eigenvalues, a sheet to one, a filament to two and a knot point to three positive eigenvalues. The sign of a given eigenvalue at a given grid node determines whether the

---

[1] Hahn et al. (2007) call the $T_{\alpha\beta}$ tensor the 'tidal tensor'. Usually, the tidal tensor is defined as the traceless part of $T_{\alpha\beta}$.

gravitational force at the direction of the corresponding eigenvector is contracting (positive eigenvalue) or expanding (negative).

Hahn et al. (2007) provided a very attractive approach to the web classification problem. It is based on the dynamical nature of the web, and so it easily lends itself to a theoretical analysis. The ease of its application to cosmological simulations opens the door for a new framework for associating the properties of galaxies and DM with environment, as defined by the web classification.

Close inspection of the Hahn et al. (2007) classification scheme and its results reveals some shortcomings. The volume filling factor for voids in Hahn et al. (2007) is very small. For their minimal smoothing scale, namely the highest resolution, the voids occupy only 17 per cent of the simulated volume. This stands in contrast to the visual impression of voids in the actual Universe and in simulations, where voids seems to occupy most of the volume but contain only a small fraction of the galaxies (in observations) or matter (in simulations). Furthermore, the Hahn et al. (2007) classification does not reproduce the visual perception of the cosmic web.

It is easy to understand the inability of the Hahn et al. (2007) approach to reproduce the visual impression. The web classification is based on the algebraic sign of the eigenvalues of the deformation tensor, namely the number of eigenvalues larger than a threshold value of zero. It follows that if an eigenvalue is only infinitesimally positive, the scheme assumes that the local neighbourhood of the given grid point collapses along the corresponding eigenvector. Yet, the collapse proceeds over the dynamical time-scale and if the value of the eigenvalue is small enough the collapse will occur, if at all, only in the distant future. Visual inspection would not classify the region as collapsing at the present time. This leads us to consider an alternative approach, namely asking the eigenvalues to be larger than a positive threshold.

Noting that the dimensionality of the deformation tensor is [time]$^{-2}$, its eigenvalues can be associated with the collapse time. It follows that the threshold value should be roughly determined by equating the collapse time with the age of the universe. This implies, however, that a separate threshold value should be determined for the one-, two- and three-dimensional collapse. Here, we will look for one threshold that characterizes the whole cosmic web. When casted in a dimensionless way (Appendix A), we expect the threshold to be of the order of unity. For an isotropic collapse, $\lambda_{th}$ can be calculated explicitly (see equations A3–A7). However, this should be taken only as a reference value and not be considered as an appropriate approximation. Rather, a phenomenological approach is adopted here and the threshold is to be determined by visual and percolation analysis of numerical simulations.

# 3 *N*-BODY SIMULATION, NUMERICAL IMPLEMENTATION AND OBJECT DETECTION

We use two numerical simulation. The first assumes a *Wilkinson Microwave Anisotropy Probe 3* (*WMAP*3) cosmology (Spergel et al. 2007) with a matter density $\Omega_m = 0.24$, a cosmological constant $\Omega_\Lambda = 0.76$, a dimensionless Hubble parameter $h = 0.73$, a spectral index of primordial density perturbations $n = 0.96$ and a normalization of $\sigma_8 = 0.76$. A simulation of box size $160\,h^{-1}$ Mpc and $1024^3$ particles has been used, corresponding to a particle mass of $3.5 \times 10^8\,M_\odot$. Starting at redshift $z = 30$, the evolution is followed using the MPI version of the Adaptive Refinement Tree (ART) code described in Gottlöber & Klypin (2008). The simulation used here is a constrained simulation of the local universe which is to be described at length in the forthcoming paper (Yepes et al., in

preparation). This is an updated and higher resolution version of the constrained simulation presented in Klypin et al. (2003). Here, the simulation is treated as random and its constrained nature is completely ignored.

In order to estimate cosmic variance effects, we have used a numerical simulation of box size $1\,h^{-1}$ Gpc. The assumed cosmology for this simulation is *WMAP*3 with a matter density $\Omega_m = 0.27$, a cosmological constant $\Omega_\Lambda = 0.73$, a dimensionless Hubble parameter $h = 0.70$, a spectral index $n = 0.95$, a normalization $\sigma_8 = 0.79$ and $1024^3$ particles corresponding to a particle mass of $9.8 \times 10^{10}\,M_\odot$. The simulation was performed using the ART code as well.

The analysis of the simulations proceeds as follows. The density field of the $160\,h^{-1}$ Mpc simulation is calculated from the particle distribution on a $256^3$ grid using the cloud-in-cell (CIC) scheme, it is then smoothed with a Gaussian kernel of width $R_s$ and from which the deformation tensor is calculated directly, using an FFT solver taking advantage of the periodic boundary conditions of the simulated volume. The deformation tensor is then diagonalized on the grid. The web characteristic of each grid point is determined by the number of eigenvalues, at that grid node, above the threshold. It should be realized that the classification is local by its nature, but the combined effect of all grid points results in the geometrical construction defined as the cosmic web.

It is important to note that the actual smoothing scale depends on both the Gaussian smoothing scale $R_s$ and the grid size $R_g$. The effective smoothing equals to $R_{eff} = \sqrt{R_s^2 + R_g^2}$. In the text, we quote always the effective smoothing.

In the $1\,h^{-1}$ Gpc simulation, we followed the same procedure, interpolating first the density on a $512^3$ grid and performing the FFT over the full volume using its periodic boundary conditions. Once the environment detection procedure is done, we select $6^3$ distinct subboxes of $160\,h^{-1}$ Mpc on a side to test the effect of cosmic variance. Fig. 1 shows the CIC density field and the cosmic web evaluated at the threshold values of $\lambda_{th} = 0.00, 0.20, 0.40, 1.00$ and $2.00$. The web is presented by a grey scale corresponding to the four web types, it is evaluated at a Gaussian effective smoothing of $R_{eff} = 0.88\,h^{-1}$ Mpc (Fig. 1). The density field and the cosmic web are evaluated on a plane of the CIC grid. Visual inspection of the density field reveals a network of voids, filaments and dense knots. The density field is evaluated on a thin plane and therefore no clear distinction can be made between the three-dimensional filaments and sheets.

The web defined by $\lambda_{th} = 0.0$ consists of many small isolated voids that occupy only a small fraction of the total area of the plane. Only as $\lambda_{th}$ increases the voids get bigger and connected and they become the dominant geometrical component of the web.

The non-zero threshold classification provides a better visual match to the density field than the null case. A qualitative analysis and comparison is presented in Section 4. The analysis is based on two quantities: the volume occupied by each web type [volume filling fraction (VFF)] and the fraction of mass contained in such a volume [mass filling fraction (MFF)].

A characterization of the cosmic web is obtained by grouping, using a FoF algorithm, neighbouring grid points of a given web type into individual objects. The FoF association proceeds in the following way: the centres of the cells in the grid are used as the position of four different kinds of cells according to its web type, then a standard FoF (Davis et al. 1985) is run over cells of the same kind with a linking length $b = 1.1$ times the grid length. Thus, only the six closest neighbours of a given cell are taken into account. The FoF void
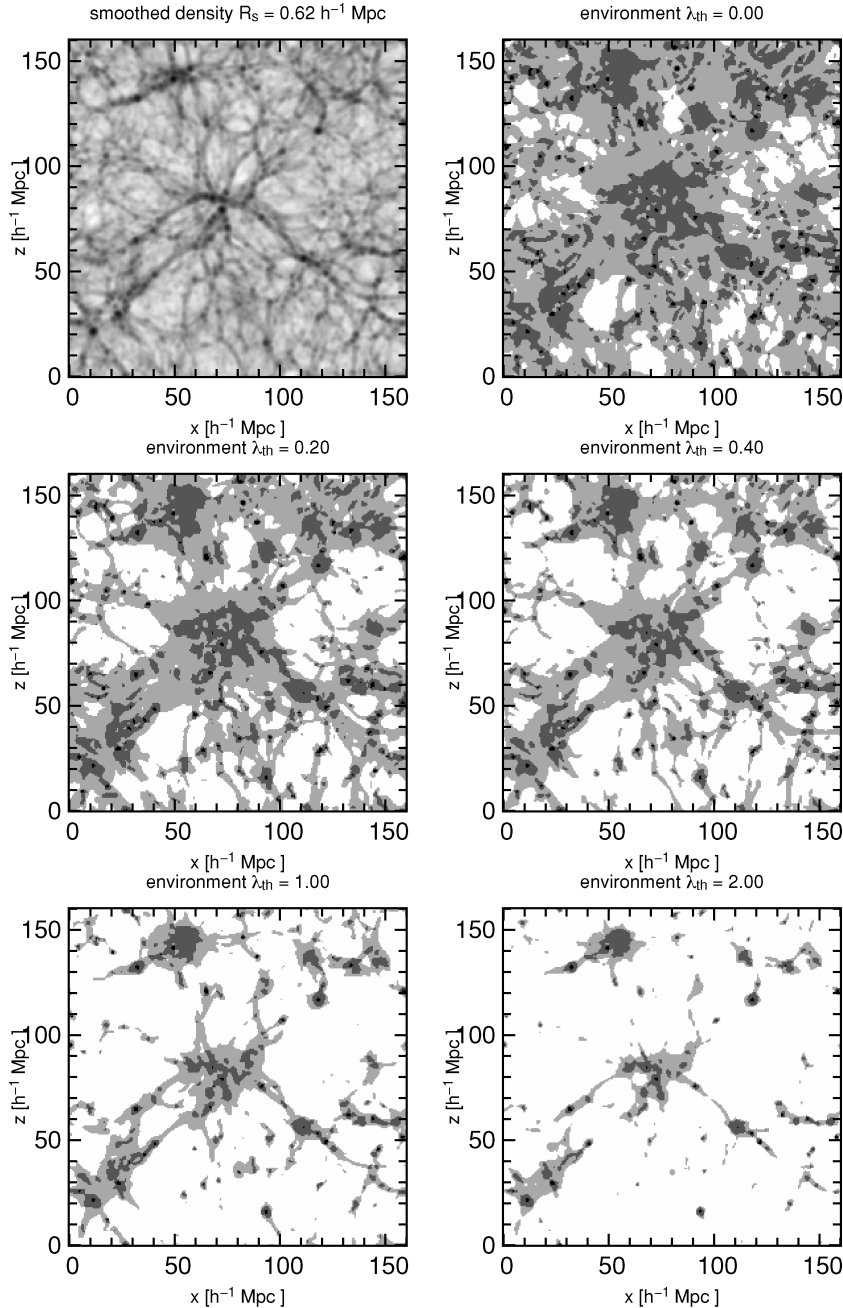
**Figure 1.** The density field and five different environmental classifications. Upper-left panel: slice of width $0.625\,h^{-1}$ Mpc depicting the density field in the simulation smoothed over a scale of $R_{\mathrm{eff}} = 0.88\,h^{-1}$ Mpc, the colour coding is logarithmic in the density – high-density peaks are dark. The other panels show the environment classification using different values for the threshold, $\lambda_{\mathrm{th}} = 0.0, 0.20, 0.40, 1.0$ and $2.0$. White corresponds to voids, clear grey to sheets, dark grey to filaments and black to knots. The general impression is that the non-zero values of $\lambda_{\mathrm{th}}$ below 1.0 capture better the environment seen by eye in the density plot.

detection is done for different simulations: the $160\,h^{-1}$ Mpc simulation, the $1\,h^{-1}$ Gpc simulation and 216 subboxes of $160\,h^{-1}$ Mpc on a side extracted from the largest simulation.

The full $160\,h^{-1}$ Mpc and $1\,h^{-1}$ Gpc computational boxes have periodic boundary conditions, but the distinct subboxes of course do not obey such boundary conditions. The FoF analysis is performed by *neglecting* the periodic boundary conditions, so as to keep a consistent analysis of all the case considered here.

The FoF algorithm is used to detect voids for different threshold values in the different simulations which are smoothed with the same physical scale $R_{\mathrm{s}} = 1.95\,h^{-1}$ Mpc, resulting in an effective resolution of $R_{\mathrm{eff}} = 2.75\,h^{-1}$ Mpc for the $1\,h^{-1}$ Gpc box and $R_{\mathrm{eff}} = 2.05\,h^{-1}$ Mpc for the $160\,h^{-1}$ Mpc box. This difference is not significant in terms of the VFF and allows for a fair comparison for the detected voids and filaments. In Section 5, a detailed analysis on these voids is presented, paying special attention to its percolation properties as the threshold rises. The same kind of analysis is

performed for the filaments in Section 6, but only on the $1\,h^{-1}$ Gpc simulation.

## 4 VOLUME AND MASS FILLING FRACTIONS

The web classification depends on two parameters that determine the environment. The first is the smoothing scale $R_{\text{eff}}$ and the second is the threshold for the eigenvalues $\lambda_{\text{th}}$. The dependency of the VFF and MFF on these two parameters is studied here. This is done for the four web types.

The VFF and MFF are measured for the four web types. First, by fixing $\lambda_{\text{th}} = 0$ and varying the smoothing scale $R_{\text{eff}}$ between $0.88\,h^{-1}$ Mpc and $12.4\,h^{-1}$ Mpc. This is also done by fixing the smoothing scale to $2.05\,h^{-1}$ Mpc and varying $\lambda_{\text{th}}$ between 0 and

1 with steps of 0.1. The results of these two cuts are shown in Fig. 2. The VFF and MFF of the case $\lambda_{\text{th}} = 0.0$ and 1.0, with two different smoothing scales $R_{\text{eff}} = 0.88$ and $2.05\,h^{-1}$ Mpc, are presented in Table 1. The evolution of the filling fraction with $\lambda_{\text{th}} = 0$ reproduces the asymptotic results expected for large smoothing scales, which is 0.42 for sheets and filaments and 0.08 for voids and knots (Doroshkevich 1970).

The most striking feature that emerges from Fig. 2 is that of the strong dependence of VFF and MFF of the voids on $\lambda_{\text{th}}$. This is to be contrasted with the other web types which show quite a similar behaviour with the change of the smoothing and the change of the threshold. It follows that the voids can serve as a sensitive monitor and indicator of the cosmic web. For the case of a null threshold, the dependence on the smoothing length is weak. The increase of $R_{\text{eff}}$
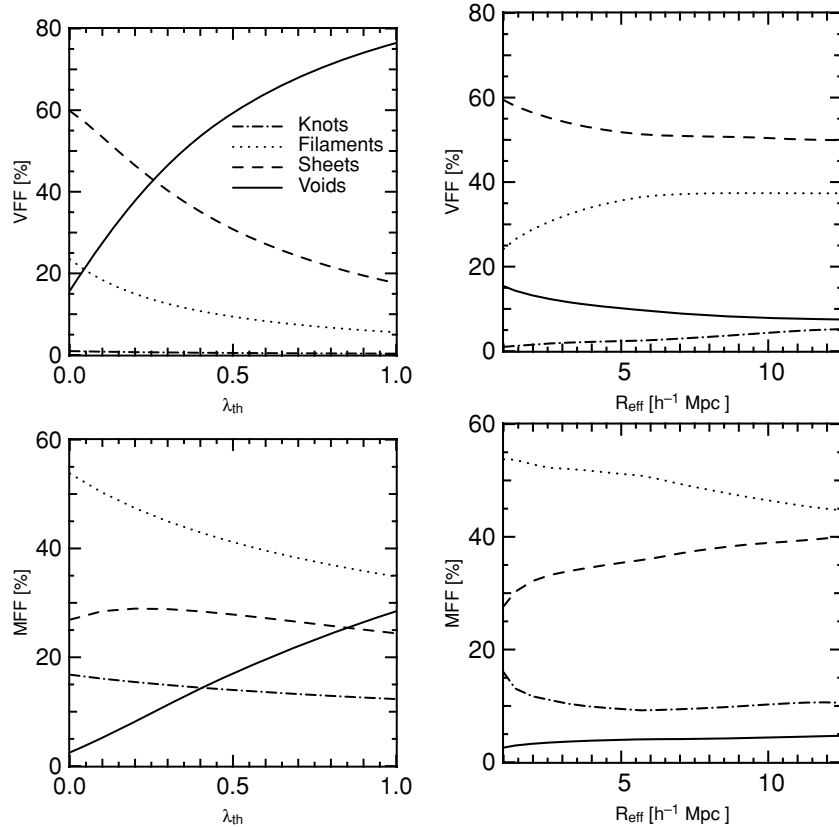
**Figure 2.** Upper panels: the VFF of knots, filaments, sheets and voids as a function of the smoothing scale $R_{\text{eff}}$ for $\lambda_{\text{th}} = 0.0$ (left-hand panel) and as a function of $\lambda_{\text{th}}$ for $R_{\text{eff}} = 2.05\,h^{-1}$ Mpc (right-hand panel). Continuous line: voids, dashed: sheets, dotted: filaments, dot–dashed: knots. Lower panels: same as the upper panel but for the MFF.

**Table 1.** VFF and MFF for the four web types for two different smoothing scales, $R_{\text{eff}} = 0.88$ and $2.05\,h^{-1}$ Mpc.

| | $R_{\text{eff}} = 0.88\,h^{-1}$ Mpc | | | | $R_{\text{eff}} = 2.05\,h^{-1}$ Mpc | | | |
| | $\lambda_{\text{th}} = 0.0$ | | $\lambda_{\text{th}} = 1.0$ | | $\lambda_{\text{th}} = 0.0$ | | $\lambda_{\text{th}} = 1.0$ | |
| Web type | Volume | Mass | Volume | Mass | Volume | Mass | Volume | Mass |
|---|---|---|---|---|---|---|---|---|
| Void | 0.16 | 0.02 | 0.76 | 0.28 | 0.13 | 0.03 | 0.82 | 0.47 |
| Sheet | 0.60 | 0.27 | 0.18 | 0.25 | 0.56 | 0.32 | 0.14 | 0.25 |
| Filament | 0.24 | 0.54 | 0.05 | 0.35 | 0.28 | 0.52 | 0.04 | 0.22 |
| Knot | 0.01 | 0.16 | 5.0e-3 | 0.12 | 0.01 | 0.11 | 2.8e-3 | 0.06 |

*Note.* For each smoothing, two extreme values of the threshold are used, $\lambda_{\text{th}} = 0.0$ and 1.0. The VFFs are similar for the same values of the threshold $\lambda_{\text{th}}$ regardless of which smoothing scale is used.
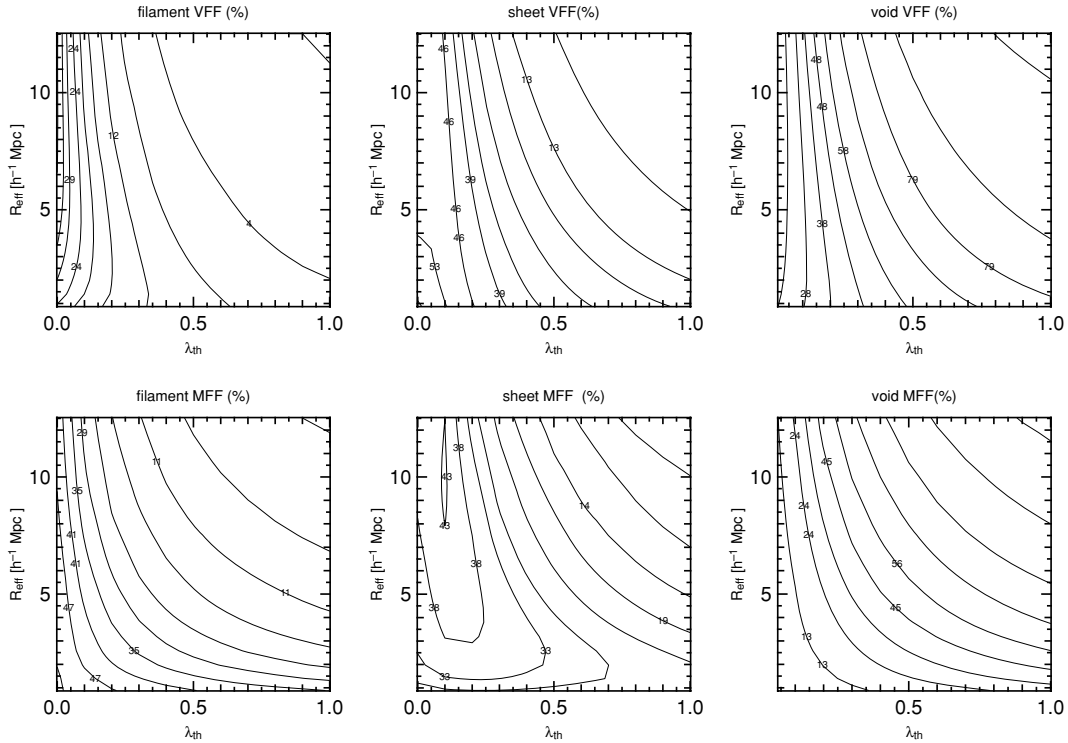
**Figure 3.** Upper row: isocontours for the VFFs for the different kinds of environment, in the plane $R_{eff} - \lambda_{th}$. Lower row: isocontours for the MFFs for the different kinds of environment, in the plane $R_{eff} - \lambda_{th}$. In both rows, from left- to right-hand panels: filaments; sheets and voids. The label on each isocontour is the percentage of the total volume filled by a given kind of environment.

corresponds to a transition to the linear regime where the density field is closer to be Gaussian.

We then perform an exploration of the space $\lambda_{th} - R_{eff}$ by making the environment classification with steps of $\Delta\lambda_{th} = 0.1$ for each smoothed density field. We measure the filling fractions for each couple $R_{eff} - \lambda_{th}$. The results are shown in Fig. 3. The important result here is that in the range of explored values the threshold on the eigenvalues is more important than the smoothing scale to fix the VFF.

Inspection of the behaviour of the VFF and MFF in the $R_{eff} - \lambda_{th}$ plane reveals that voids on the one hand and the sheets and filaments on the other are complementing each other. This means that the VFF and MFF for voids increases with both $R_{eff}$ and $\lambda_{th}$ at expenses of the volume and mass in sheets and filaments.

This provides more evidence for the distinct nature of voids. The VFF of the voids, sheets and filaments clearly show the significance of the $\lambda_{th} \lesssim 0.2$ case. For that threshold, the contour lines are almost vertical, implying that the VFF of these web elements are almost independent of $R_{eff}$. The MFF, on the other hand, distinguishes very easily different values of the smoothing scale $R_{eff}$.

## 5 PERCOLATION OF VOIDS

Here, we focus on the analysis of the statistical distribution of the sizes of the voids and their percolation. The emphasis on voids does not stem only from the extensive work done on their properties (Colberg et al. 2008) but also because they constitute the most sensitive gauge of the cosmic web and its dependence on the threshold of the eigenvalues.

A simplified characterization was already performed in Section 4 by measuring the volume and mass occupied in the void environment. Here, the dependence of the number of voids and their perco-

lation properties on $\lambda_{th}$ is examined. The percolation is quantified by the fraction of volume of the largest (in volume) void ($V_{max}$) to the total volume occupied by all voids ($V_{tot}$).

The void identification is performed here at a fixed smoothing scale, $R_{eff} = 2.75$ and $2.05\,h^{-1}$ Mpc for the $1\,h^{-1}$ Gpc and $160\,h^{-1}$ Mpc, respectively, and by varying the eigenvalues threshold in the range of $0 < \lambda_{th} < 0.3$. Fig. 4 (left-hand panel) shows that the number of voids in the simulation decays roughly exponentially with $\lambda_{th}$, $N_{void} = N_0\exp(-\lambda_{th}/\lambda_D)$, where $N_0$ is the number of voids for the null threshold and $\lambda_D$ is a typical scale over $\lambda_{th}$ to quantify the decay in the number of voids.

Fig. 4 (right-hand panel) presents the fraction of the volume of the largest (in volume) void to the total volume of all the voids ($V_{max}/V_{tot}$). A transition occurs between $0.1 \lesssim \lambda_{th} \lesssim 0.2$ where the ratio jumps from $\leq 0.1$ to $\geq 0.9$. Note that the percolation starts at the stage in which the VFF of voids is only $\sim 25$ per cent. It follows that in spite of the small VFF obtained for $\lambda_{th} \sim 0.1$ the voids start to coalesce and form one supervoid which encompasses 90 per cent of the total volume of voids when the void VFF reaches 60 per cent. As we will show in Section 7, this transitional scale is dependent on the particular simulation under consideration.

The percolation analysis depends on the boundary conditions of the studied volumes. Two distinct cases of boundary conditions are presented in Fig. 4. One corresponds to the ensemble of sub-boxes cut out from the $1\,h^{-1}$ Gpc computational box, in which the boundary conditions are left free. The other is the case of the full computational boxes which obey periodic boundary conditions. In both cases, the FoF analysis is performed by neglecting the possibility of periodic boundary conditions. Evidently, the first case better corresponds to the actual astronomical case in which a percolation analysis would be applied to finite volumes with boundary free conditions. Fig. 4 clearly show that the percolation curves of the two
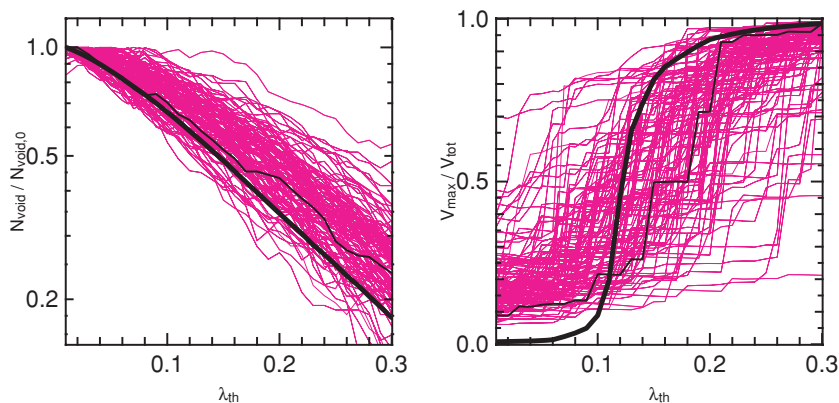
**Figure 4.** Percolation results. Left-hand panel: number of voids as a function of the threshold in eigenvalues normalized to the number of voids at $\lambda_{th} = 0.0$. A fixed smoothing of $R_s = 1.95\,h^{-1}$ Mpc is used here for all the simulations. It corresponds to $R_{eff} = 2.75$ and $2.05\,h^{-1}$ Mpc for the $1\,h^{-1}$ Gpc and $160\,h^{-1}$ Mpc simulation, respectively. The thick line shows the results for the $1\,h^{-1}$ Gpc simulation, the thin line shows the results for the $160\,h^{-1}$ Mpc simulation. The magenta lines show the results for the subvolumes extracted from the $1\,h^{-1}$ Gpc simulation. Right-hand panel: fraction of the total void volume occupied by the largest void. The line coding is the same as in the left-hand panel. Results from the large $1\,h^{-1}$ Gpc differ greatly from the results in the simulation $160\,h^{-1}$ Mpc, nevertheless the later is consistent within the scatter deduced from the subvolumes. Even when it is clear that the detailed shape of the curve depends on the simulation size, it seems to be a robust feature that the largest change in the supervoid size is presented around $0.1 \lesssim \lambda_{th} \lesssim 0.2$.

full boxes lie within the variance spanned by the subboxes, suggesting the dynamical effect of the boundary conditions lies within the cosmic variance.

The question of how the incorporation of the periodic boundary conditions into the FoF analysis affects the percolation analysis is interesting, even if it is somewhat 'academic'. A simple reasoning suggests that this causes the systems to percolate at smaller $\lambda_{th}$. Percolation is defined as the point where $V_{max}/V_{tot}$ exceeds a certain value. Now, the incorporation of the periodic boundary conditions does not change $V_{tot}$ but it connect voids, that are otherwise not connected and hence $V_{max}$ increases. It follows that this reduces the percolation threshold. Furthermore, the smaller is the computational box the larger is the effect. We have found that by including periodic boundary conditions in the analysis the percolation threshold drops by 0.10 and 0.05 for the $160\,h^{-1}$ Mpc and $1\,h^{-1}$ Gpc boxes, respectively.

# 6 FRAGMENTATION OF FILAMENTS

Along with voids, filaments have received some attention in the literature as a natural way to probe large-scale structure (Novikov et al. 2006; Sousbie et al. 2008). A study of the filaments is performed here, focusing on their percolation dynamics.

As opposed to voids, filaments start to fragment as the threshold $\lambda_{th}$ is raised. This is clear in Fig. 1, which shows that the filaments disappear as $\lambda_{th}$ increases, making room for the growing voids.

Consequently, one could expect that for some range of $\lambda_{th}$ there are two coexisting environments: a complex of percolating voids and a network of interconnected filaments, something close to the visual impression of the comic web. The percolation analysis of the filament and void networks can help to define an interval of $\lambda_{th}$ values where the environment studies would be feasible.

The percolation analysis of filaments is applied here to the $1\,h^{-1}$ Gpc simulation. Fig. 5 shows the ratio of the volume of largest filament to the total volume occupied by filaments plotted together with $V_{max}/V_{tot}$ for the voids (presented also in the right-hand panel of Fig. 4). The filament fraction evolves from a value close to ~1 for $\lambda_{th} = 0.0$ down to values close to zero for $\lambda_{th} \sim 1.5$. It confirms
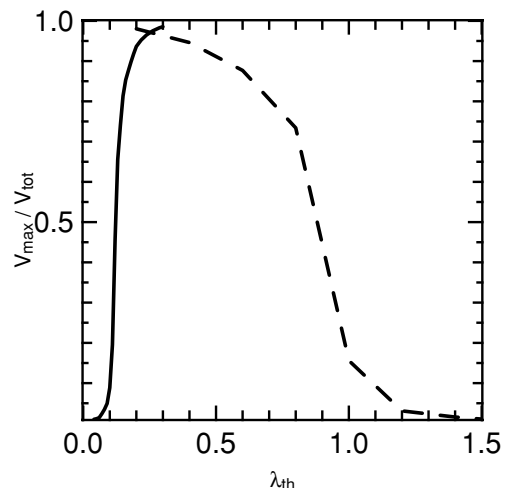


**Figure 5.** The continuous line shows the fraction of total volume in voids occupied by the largest void. The dashed line shows the fraction of the total volume in filaments occupied by the largest filament. Both curves refer to the $1\,h^{-1}$ Gpc simulation. As the eigenvalue threshold rises, the voids percolate, while the network of filaments fragments. The two fractions are the same at $\lambda_{th} = 0.25$.

the visual intuition we had of a fully interconnected network of filaments that fragments as the eigenvalue threshold increases.

The percolation/fragmentation curves intersect at $\lambda_{th} = 0.25$, when the two fractional volumes are ~97 per cent. Heuristically, one can assume a given network to exist, namely percolate, when its fractional volume exceeds 95 per cent. The web is then defined at the threshold level at which the voids and filaments networks coexist. This implies a threshold interval of $0.20 \lesssim \lambda_{th} \lesssim 0.40$. Such a heuristic approach is in a good agreement and matches the visual impression of the LSS (Fig. 1). This approximate interval should hold for lower smoothing scales, as the VFF (our gauge for the percolation dynamics) is almost independent of the smoothing scale for the range of thresholds considered, as seen in Fig. 3, and suggested as well in the values of Table 1.

Again, the incorporation of periodic boundary conditions in the analysis changes the interval in $\lambda_{th}$ where the interconnected voids and filaments coexist. However, the effect decreases with the size of the computational box. In the case of the $1\,h^{-1}$ Gpc simulation, the intersection of the percolation and fragmentation curves moves by a mere $\Delta\lambda_{th} = 0.01$. In the $160\,h^{-1}$ Mpc simulation, the intersection changes from $\lambda_{th} = 0.30$ in the absence of periodic boundary conditions to $\lambda_{th} = 0.25$ when periodicity is included. In both cases, the fractional volumes at intersection are larger than $\sim95$ per cent.

## 7 SIMULATION BOX SIZE AND COSMIC VARIANCE

The dependence of the cosmic web classification on the cosmic variance and the simulation box size is further studied here. This is done by analysing the VFF and the MFF in the three following cases.

(i) The $1\,h^{-1}$ Gpc simulation with its density field evaluated on a $512^3$ grid and Gaussian smoothed with $R_s = 1.95\,h^{-1}$ Mpc, making $R_{eff} = 2.75\,h^{-1}$ Mpc.

(ii) The $160\,h^{-1}$ Mpc simulation with a $256^3$ grid density field smoothed with $R_s = 1.95\,h^{-1}$ Mpc, making $R_{eff} = 2.05\,h^{-1}$ Mpc .

(iii) $6^3$ distinct subboxes of the $1\,h^{-1}$ Gpc simulation, with the same smoothing and grid cell as the $1\,h^{-1}$ Gpc simulation. The ensemble of 216, $160\,h^{-1}$ Mpc subboxes is used to study the effect of cosmic variance.

Fig. 6 shows the result for the VFF and MFF. The results for the $160\,h^{-1}$ Mpc simulation are well within the variance calculated

from the subvolumes in the $1\,h^{-1}$ Gpc simulation. In the case of the MFF, the result for the $160\,h^{-1}$ Mpc are located far from the mean value in the $1\,h^{-1}$ Gpc, nevertheless it is located within the dispersion defined by the subvolumes. In general, the VFF and MFF are consistent in all the three kinds of simulations. The agreement is less impressive than with the VFF, perhaps as well due to the different values of the effective smoothing scale $R_{eff}$. From the results in Fig. 3, we know that the smoothing plays a more important role in the MFF than in the VFF, especially for high values of $\lambda_{th}$.

The growth of the largest void in the simulation, Fig. 4, is very different between the three kinds of simulations. The fraction of void volume occupied by the supervoid is very dependent on the simulation size. For the large $1\,h^{-1}$ Gpc simulation, the initial values of $V_{max}/V_{tot}$ for $\lambda_{th} = 0.0$ are the lowest possible, this can be readily understood by the fact that $V_{tot}$ grows with the simulation box size, while the volume of the largest void, $V_{max}$, is of the same order of magnitude regardless of the simulation size. For values larger than $\lambda_{th} = 0.2$, the large simulation has almost percolated into a single supervoid, while the subvolumes still show a large dispersion in their percolation behaviour. The results for the small $160\,h^{-1}$ Mpc simulation are consistent with such dispersion. In spite of this, in all the three cases there is a clear transitional behaviour starting at $\lambda_{th} = 0.1$ and finishing around $\lambda_{th} = 0.2$, even when the detailed behaviour with $\lambda_{th}$ is far from being the same.

## 8 CONCLUSIONS

This paper presents an algorithm for classifying the cosmic web and its application to pure DM simulations. The scheme is based on
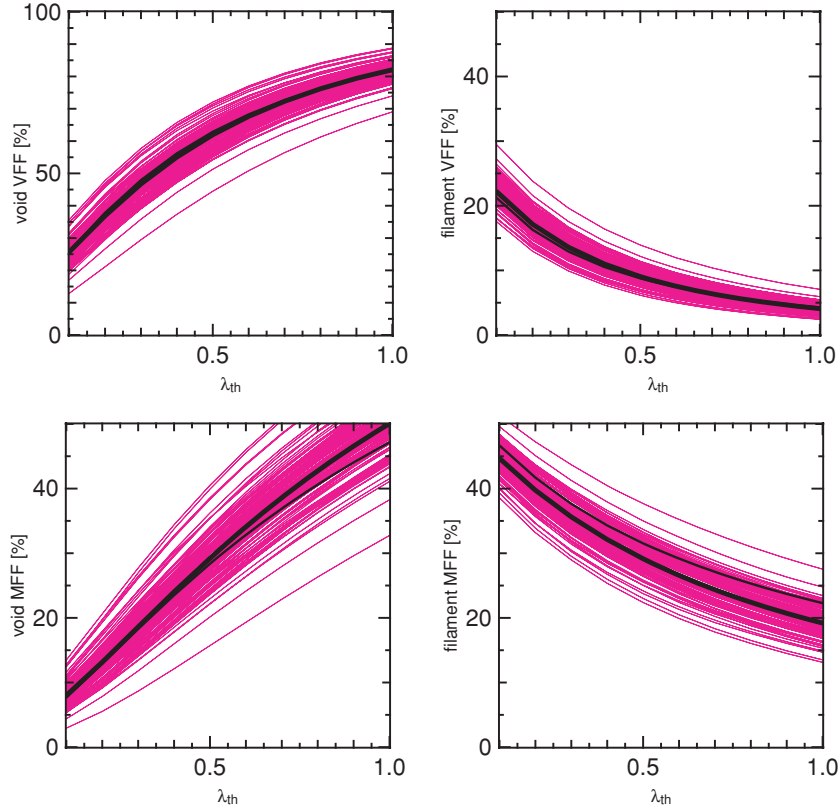


**Figure 6.** Cosmic variance effects on volume and MFFs for voids and filaments. Thick black line: simulation $1\,h^{-1}$ Gpc, thin black line: simulation $160\,h^{-1}$ Mpc, magenta lines: subvolumes extracted from the $1\,h^{-1}$ Gpc simulation. Upper panels: VFF of voids (left-hand panel) and filaments (right-hand panel) as a function of the eigenvalue threshold $\lambda_{th}$. Lower panels: same as the upper panels for the MFFs.

the analysis of the Hessian of the gravitational potential generated by the DM distribution. The algorithm presented here constitutes an improvement on the scheme of Hahn et al. (2007), involving a pertinent reinterpretation of the dynamics in the problem. This is achieved by relaxing the $\lambda_{th} = 0$ assumption of Hahn et al. and recognizing the fact that $\lambda_{th}$ is related to the collapse time-scale. This improvement allows a more realistic treatment of the cosmic web.

Inspection of the different plots of Fig. 2 reveals the striking difference in the way the cosmic web, and in particular the voids, responds to the changes in the Gaussian smoothing and the $\lambda_{th}$'s threshold. Keeping a null $\lambda_{th}$ and changing $R_{eff}$, we see that the non-linear evolution does not change the ranking of the VFF and MFF found in the deep linear regime (i.e. $R_{eff} \approx 12.5 \, h^{-1}$ Mpc). Namely, for the null threshold the sheets have the highest VFF and the filaments the highest MFF, independent of $R_{eff}$. Considering the case of a fixed $R_{eff} = 2.05 \, h^{-1}$ Mpc, the void VFF grows strongly with $\lambda_{th}$ and above $\lambda_{th} \sim 0.5$ the voids have the highest VFF. The results on the VFF are extremely robust with respect to the simulation size and cosmic variance effects. In the case of the void MFF, it changes from the lowest one at $\lambda_{th} = 0$ to the second highest at $\lambda_{th} = 1.0$.

The nature of the web changes dramatically with the threshold as it becomes volume dominated by the voids as $\lambda_{th}$ increases. The MFF shows a larger cosmic variance, compared with the VFF. Also, it is equally sensitive to changes in the smoothing scale and the threshold value.

The web classification provides a set of flagged points on a grid, and the collection of neighbouring grid points of a given environmental type, connected by an FoF algorithm, forms objects we associate with voids, sheets, filaments and knots. The statistical properties of the system of voids and their dependence on $\lambda_{th}$ have been explored here. In particular, the number of isolated voids and their sizes have been analysed, finding that the number of isolated voids roughly decreases exponentially with $\lambda_{th}$. In the $1 \, h^{-1}$ Gpc simulation, the system of voids percolates between $0.1 \lesssim \lambda_{th} \lesssim 0.2$, at which the largest void jumps from having less than 10 per cent to 90 per cent of the volume occupied by voids. The percolation dynamics is also seen on average in the different smaller simulations, with a wide spread of observed percolation, but keeping the same threshold interval for the transition.

The association of the eigenvectors of the deformation tensor with the collapse time, and hence with the age of the universe, enables in principle a theoretical determination of $\lambda_{th}$. A thorough analysis would have yielded a threshold value that depends on the dimensionality of the collapse. A fiducial or a reference value is provided by the spherical collapse model in the *WMAP*3 cosmology of $\lambda_{th} = 3.21$. However, at that high value the web (in particular the network of filaments) looks very fragmented. The application of the ellipsoidal collapse model (Sheth & Tormen 2002) might provide a better theoretical estimate.

Short of a 'first principle' determination of $\lambda_{th}$ we resort to a heuristic approach. We look for the range of $\lambda_{th}$ over which the percolated networks of the voids and filaments coexist for a fixed smoothing scale of $R_{eff} = 2.75 \, h^{-1}$ Mpc in the $1 \, h^{-1}$ Gpc simulation. The voids and filaments behave in an opposite way in terms of the dependence of the percolation on the threshold value. At low $\lambda_{th}$, the voids are isolated and the filaments percolated and at high $\lambda_{th}$ the voids percolate and the filaments fragment. Adopting a 95 per cent in the fractional volume as defining the percolation transition, we find the web to be defined by a threshold in the range of $0.20 \lesssim \lambda_{th} \lesssim 0.40$. This range stands in good agreement with the visual impression obtained from the simulations.

The notion of the cosmic web is not new. The filamentary structure has been extensively studied, mostly within the context of the Zeldovich pancakes (Zeldovich 1970). The role of voids has also been heavily studied and many algorithms for voids finding have been suggested (see Colberg et al. 2008). We have been motivated by the computational simplicity and the elegance of the Hahn et al. (2007) approach and have modified it in a way that reproduces the web as it emerges from observations and simulations. Our main drive is to provide a simple, fast and precise tool for classifying the environmental properties of each point in space. Using the non-zero thresholding of the eigenvalues of the Hessian of the potential indeed provides a very efficient tool that can be easily applied to simulations. The same analysis can be performed at different red-shifts in the simulation, allowing the classification of environment as a function of time.

A key problem in cosmology and structure formation is the role of environment in the formation of galaxies. A related question is to what extent the properties of galaxies forming within a DM halo are determined only by the halo mass. It is important to examine the possibility that direct environmental factors do affect galaxy formation, and a mathematical language describing the environment is a necessity in such an endeavour. Our main drive has been the need for an algorithm that provides a clear and intuitive classification of the cosmic web that can be easily incorporated into galaxy formation models. We think that the web classification method presented here indeed fulfills that need and that it can be readily incorporated into semi-analytical schemes of galaxy formation.

## REFERENCES

Aragón-Calvo M. A., Jones B. J. T., van de Weygaert R., van der Hulst J. M., 2007, A&A, 474, 315
Arbabi-Bidgoli S., Müller V., 2002, MNRAS, 332, 205
Arnold V. I., Shandarin S. F., Zeldovich I. B., 1982, Geophys. Astrophys. Fluid Dyn., 20, 111
Avila-Reese V., Colín P., Gottlöber S., Firmani C., Maulbetsch C., 2005, ApJ, 634, 51
Blanton M. R., Eisenstein D., Hogg D. W., Schlegel D. J., Brinkmann J., 2005, ApJ, 629, 143
Bond J. R., Kofman L., Pogosyan D., 1996, Nat, 380, 603
Brunino R., Trujillo I., Pearce F. R., Thomas P. A., 2007, MNRAS, 375, 184

Colberg J. M., Sheth R. K., Diaferio A., Gao L., Yoshida N., 2005, MNRAS, 360, 216

Colberg J. M. et al., 2008, MNRAS, 387, 933

Davis M., Efstathiou G., Frenk C. S., White S. D. M., 1985, ApJ, 292, 371

Doroshkevich A. G., 1970, Astrophys., 6, 320

Dressler A., 1980, ApJ, 236, 351

Gao L., Springel V., White S. D. M., 2005, MNRAS, 363, L66

Gottlöber S., Klypin A., 2008, in Wagner S., Steinmetz M., Bode A., Brehm M., eds, High Performance Computing in Science and Engineering, The ART of Cosmological Simulations. Springer-Verlag, Berlin, p. 29

Gottlöber S., Łokas E. L., Klypin A., Hoffman Y., 2003, MNRAS, 344, 715

Hahn O., Porciani C., Carollo C. M., Dekel A., 2007, MNRAS, 375, 489

Klypin A. A., Shandarin S. F., 1983, MNRAS, 204, 891

Klypin A., Hoffman Y., Kravtsov A. V., Gottlöber S., 2003, ApJ, 596, 19

Lee J., Lee B., 2008, ApJ, 688, L78

Lemson G., Kauffmann G., 1999, MNRAS, 302, 111

Maulbetsch C., Avila-Reese V., Colín P., Gottlöber S., Khalatyan A., Steinmetz M., 2007, ApJ, 654, 53

Neyrinck M. C., 2008, MNRAS, 386, 2101

Novikov D., Colombi S., Doré O., 2006, MNRAS, 366, 1201

Platen E., van de Weygaert R., Jones B. J. T., 2007, MNRAS, 380, 551

Plionis M., Basilakos S., 2002, MNRAS, 330, 399

Shandarin S., Feldman H. A., Heitmann K., Habib S., 2006, MNRAS, 367, 1629

Sheth R. K., Tormen G., 2002, MNRAS, 329, 61

Sousbie T., Pichon C., Colombi S., Novikov D., Pogosyan D., 2008, MNRAS, 383, 1655

Spergel D. N. et al., 2007, ApJS, 170, 377

White S. D. M., Rees M. J., 1978, MNRAS, 183, 341

Zeldovich Y. B., 1970, A&A, 5, 84

## APPENDIX A: SETTING THE THRESHOLD FOR WEB CLASSIFICATION

In this paper, we use the eigenvalues of the deformation tensor, equation (1), normalized in a specific way. Here, we provide details of the normalization and give motivation for selecting the threshold.

We write the Poisson equation in the following form:

$$\nabla^2 \tilde{\phi} = 4\pi G \bar{\rho} \delta = \tilde{\lambda}_1 + \tilde{\lambda}_2 + \tilde{\lambda}_3, \tag{A1}$$

where $\bar{\rho}$ is the mean matter density of the universe and $\delta$ is the matter overdensity. One can rescale the gravitational potential and the eigenvalues of the deformation tensor by dividing them by $4\pi G \bar{\rho}$:

$$\nabla^2 \phi = \delta = \lambda_1 + \lambda_2 + \lambda_3. \tag{A2}$$

Note that $4\pi G \bar{\rho}$ provides a natural scale to introduce dimensionless parameters $\lambda_i$. We solve this equation numerically.

The spherical collapse model is invoked here so as to get a reference value for $\lambda_{th}$. The (spherical) free-fall time is related to the local density by

$$\tau_{ff} = \sqrt{\frac{3\pi}{32 G \rho}}. \tag{A3}$$

Recalling that

$$4\pi G \bar{\rho} = \frac{3}{2} \Omega_m H_0^2 \tag{A4}$$

(where $\Omega_m$ is the value of the cosmological matter density and $H_0$ is the Hubble constant), equation (A1) is rewritten as

$$\nabla^2 \tilde{\phi} = \tilde{\lambda}_1 + \tilde{\lambda}_2 + \tilde{\lambda}_3 = 4\pi G \rho - 4\pi G \bar{\rho}. \tag{A5}$$

The threshold can be estimated by demanding that the free-fall time equals the age of the universe ($\tau_0$). Namely, the threshold separates between the principal axes that have collapsed by $\tau_0$ and the ones that have not. Substituting the free-fall time by the age of the universe, the threshold is given by

$$3\beta(\lambda_i)\tilde{\lambda}_{th} = \frac{3\pi^2}{8\tau_0^2} - \frac{3}{2}\Omega_m H_0^2, \tag{A6}$$

where $\beta$ is a fiducial factor introduced to account for the deviation from local isotropy.

In terms of the dimensionless eigenvalues, the threshold is given by

$$\lambda_{th} = \frac{1}{3\beta(\lambda_i)} \left[ \frac{\pi^2}{4} \frac{1}{\Omega_m} (\tau_0 H_0)^{-2} - 1 \right]. \tag{A7}$$

For the *WMAP*3 parameters used in the $160\,h^{-1}$ Mpc simulation, we have $\Omega_m = 0.24$, $h = 0.73$ and $\tau_0 H_0 = 0.983$. It follows that $\lambda_{th} = 9.63/(3.0\beta)$. For the spherical case of $\beta(\lambda_i) = 1$, the threshold is $\lambda_{th} = 3.21$.

This paper has been typeset from a TEX/LATEX file prepared by the author.